Journal of the Mechanics and Physics of Solids 116 (2018) 135–149

Contents lists available at ScienceDirect

Journal of the Mechanics and Physics of Solids

journal homepage: www.elsevier.com/locate/jmps

Modal nudging in nonlinear elasticity: Tailoring the elastic post-buckling behaviour of engineering structures

B.S. Cox[a,*], R.M.J. Groh[a], D. Avitabile[b], A. Pirrera[a]

[a] Bristol Composites Institute (ACCIS), Department of Aerospace Engineering, University of Bristol, Queen's Building, University Walk, Bristol, BS8 1TR, UK
[b] School of Mathematical Sciences, University of Nottingham, University Park, Nottingham, NG7 2RD, UK

ARTICLE INFO

Article history:
Received 22 January 2018
Revised 28 March 2018
Accepted 29 March 2018
Available online 30 March 2018

Keywords:
Modal nudging
Geometric nonlinearities
Post-buckling
Imperfection sensitivity

ABSTRACT

The buckling and post-buckling behaviour of slender structures is increasingly being harnessed for smart functionalities. Equally, the post-buckling regime of many traditional engineering structures is not being used for design and may therefore harbour latent load-bearing capacity for further structural efficiency. Both applications can benefit from a robust means of modifying and controlling the post-buckling behaviour for a specific purpose. To this end, we introduce a structural design paradigm termed *modal nudging*, which can be used to tailor the post-buckling response of slender engineering structures without any significant increase in mass. Modal nudging uses deformation modes of stable post-buckled equilibria to perturb the undeformed baseline geometry of the structure imperceptibly, thereby favouring the seeded post-buckling response over potential alternatives. The benefits of this technique are enhanced control over the post-buckling behaviour, such as modal differentiation for smart structures that use snap-buckling for shape adaptation, or alternatively, increased load-carrying capacity, increased compliance or a shift from imperfection sensitivity to imperfection insensitivity. Although these concepts are, in theory, of general applicability, we concentrate here on planar frame structures analysed using the nonlinear finite element method and numerical continuation procedures. Using these computational techniques, we show that planar frame structures may exhibit isolated regions of stable equilibria in otherwise unstable post-buckling regimes, or indeed stable equilibria entirely disconnected from the natural structural response. In both cases, the load-carrying capacity of these isolated stable equilibria is greater than the natural structural response of the frames. Using the concept of *modal nudging* it is possible to "nudge" the frames onto these equilibrium paths of greater load-carrying capacity. Due to the scale invariance of modal nudging, these findings may impact the design of structures from the micro- to the macro-scale.

* Corresponding author.
E-mail addresses: Bradley.Cox@bristol.ac.uk (B.S. Cox), Rainer.Groh@bristol.ac.uk (R.M.J. Groh), Daniele.Avitabile@nottingham.ac.uk (D. Avitabile), Alberto.Pirrera@bristol.ac.uk (A. Pirrera).

https://doi.org/10.1016/j.jmps.2018.03.025
0022-5096/

1. Introduction

In structural mechanics, nonlinearities are often viewed as failure modes. In the case of material nonlinearity, where plastic deformations irreversibly change the constitutive behaviour of the material, avoiding nonlinearity is a good heuristic. On the other hand, reversible nonlinearities can be employed for additional functionality. As a typical example, elastic snap-buckling of a shallow arch can be viewed as a failure mode if the application is a footbridge, but can also be treated as a valuable mechanism for rapid and reversible shape-change in applications such as energy-harvesting devicses (Harne and Wang, 2013).

In this sense, while buckling is historically viewed as a failure event with little practical significance, exploiting buckling for smart functionality has become a prevalent theme in the literature (Hu and Burgueño, 2015a; Reis, 2015). The disciplines of micro-electromechanical systems (MEMS) (Andò et al., 2010; Bogue, 2013; Jog and Patil, 2016; Tsai and Sue, 2007); deployable, morphing and compliant structures (Arena et al., 2017; Cox et al., 2018; Gomez et al., 2017; Groh and Pirrera, 2018a; Pirrera et al., 2012; Previtali et al., 2011; Sofla et al., 2010); meta-materials (Bertoldi et al., 2010; Florijn et al., 2014; Mullin et al., 2007; Overvelde et al., 2012); and energy harvesters (Harne and Wang, 2013) are all leading the way in embracing buckling as a design tool.

Many smart applications employ bistable components for additional functionality. In this case, the buckling behaviour is binary and no additional control, beyond the applied load, is required to transition between two configurations. Alternatively, shape-adaptive components can be designed to feature a number of different stable post-buckled configurations, and in this case, a means of modal differentiation is required (Groh and Pirrera, 2018b). This is especially the case, because structures that can attain a larger number of stable configurations, such as cylindrical shells, suffer from severe imperfection sensitivity, and hence, prediction and control of the observed behaviour is challenging.

Equally, traditional engineering structures can benefit from controlling the post-buckling behaviour. A major goal of any post-buckling analysis is to differentiate between post-critical behaviour that is stable and progressive, or unstable and catastrophic. In case of the former, the structure continues to take load beyond the first instability point, but often with reduced rigidity. Furthermore, the structure can have more than one stable post-buckling response, with no guarantee that the naturally observed behaviour leads to the greatest load-carrying capacity or compliance before failure. In case of the latter, the initially unstable post-critical behaviour typically stabilises deeper into the post-critical regime, but once the structure snaps into this configuration, the load-carrying capability of the structure has often been reduced or irreversible material nonlinearity has occurred. Furthermore, the sharp two-thirds power law of the cusp catastrophe, which governs the relation between buckling load and geometric imperfections, implies a pronounced and detrimental sensitivity to imperfections (Thompson and Hunt, 1973). The combination of imperfection sensitivity and the stochastic nature of imperfections leads to uncertainty during design (Arbocz and Hol, 1995), which means that imperfection-sensitive structures, such as cylindrical shells under axial compression, are designed with empirically derived and often conservative knock-down factors (Jiménez et al., 2017).

In this vein, this paper explores the potential of controlling structural nonlinearities to tailor the post-buckling response of engineering structures for a specific purpose. Predominant in this field is the work by Mang et al. (2006) and Schranz et al. (2006) who investigated potential means of transforming imperfection-sensitive designs into imperfection-insensitive ones. Their research shows that this shift can be achieved by (i) altering the thickness of the structure; (ii) attaching auxiliary members (*e.g.* springs); and (iii) varying the geometry of the structure. Although this approach can be highly effective, it has drawbacks if certain geometrical space constraints need to be imposed, or when it is not possible to fix additional components to the structure. Ning and Pellegrino (2015) showed that the imperfection-sensitive cylindrical shell under axial compression can be transformed into an imperfection-insensitive design by changing the cross-sectional topology. In doing so, the cross-section is transformed from circular to wavy, potentially rendering the new structure geometrically less useful for operation in service.

White and Weaver (2016) introduced an interesting concept for imperfection-insensitive cylindrical shells by using the stiffness-tailoring capacity of fibre-reinforced plastic materials. By means of an optimisation framework, White and Weaver (2016) showed that laminated composites with curvilinearly varying fibre paths can be used to tailor the elastic modulus across cylindrical panels such that there is no degradation in axial stiffness in the post-buckling regime. In this manner, the typically unstable “shell-like” post-buckling response can be transformed into a more benign stable “plate-like” response. Similarly, Wu et al. (2018) used the technology of fibre-steering to tailor both the fibre orientation and thickness of composite panels under compression to optimise to an effectively “buckle-free” structure with negligible loss of axial stiffness in the post-critical regime.

Finally, Burgueño and co-workers have published extensively on tailoring the post-buckling behaviour of slender structures for smart applications. For example, the mode-jumping characteristics (number of mode jumps, load drops during mode jumping, hysteretic energy dissipation, *etc.*) in the post-buckling regime of axially compressed cylindrical shells may be controlled by patterned stiffness distributions, lateral constraints and laminate stacking sequence variations (Burgueño et al., 2014). Similarly, the elastic post-buckling response in terms of initial and final stiffness can also be tailored using modal superpositions of buckling modes seeded as initial imperfections (Hu and Burgueño, 2017). This approach is also valuable for reducing the imperfection sensitivity of axially compressed cylindrical shells (Hu et al., 2014; Hu and Burgueño, 2015b).

This paper follows a similar approach in that "imperfections by design" create opportunities for achieving a particular post-buckling response. The present approach differs in that it does not use superpositions of buckling eigenmodes as seeded imperfections, which require an optimisation procedure to find the modal combination that yields the desired response. Instead, the present approach chooses a particular desirable deformation mode from the post-buckling regime of the baseline idealised structure, and then applies this mode as an initial seed to "nudge" the structure onto this particular post-buckling path. This methodology therefore requires a comprehensive quasi-static exploration of the design space to identify desirable regions of stable equilibria. To reflect this methodology we use the term *modal nudging*, and the aim of this paper is to introduce this concept as a general design paradigm—first, as a means of converting imperfection-sensitive structures into imperfection-insensitive designs in a minimally invasive manner, and second, as a way of exploiting latent load-carrying capacity.

The rest of the paper is structured as follows. Section 2 introduces the concept of modal nudging using two planar frame structures, and presents the results of both frames with a discussion of the key findings. Section 3 introduces two additional frames, which highlight some of the limitations of modal nudging. Finally, conclusions are drawn in Section 4.

2. Modal nudging

Modal nudging is a design strategy that intends to improve the load-carrying capacity, compliance and/or stability of a structure, by nudging the structure to follow a specific equilibrium path. The term "nudging" is borrowed from *nudge theory*—recently awarded the Nobel prize in economic sciences (Thaler, 2015; Thaler and Sunstein, 2009), common also in political theory (Leggett, 2014) and behavioural science (Voyer, 2015)—where small suggestions are used to elicit non-forced compliance in individuals.

Modal nudging is a simple-to-employ method akin to applying a specific geometric imperfection to the original, stress-free geometry of a structure. In structural mechanics, imperfections traditionally relate to small stochastic deviations from an idealised model geometry that are credited for drastically reducing the experimentally observed buckling loads of post-critically unstable structures. Modal nudging differs from this traditional definition in that the small geometric changes applied to the structure are (i) deterministically chosen and imposed with intent; and (ii) do not lead to an impaired version of the idealised behaviour, but to an entirely new structural response. In this regard, the geometric changes imposed by modal nudging cannot be viewed as the inevitable imperfections of reality, but rather as chosen design features, which nonetheless, remain negligibly small compared to the original geometry. In this manner, a nudge may be described as a non-random, yet small, initial perturbation.

A particular nudge mode is chosen from information gathered about the post-buckled regime of the baseline idealised structure. A comprehensive exploration of the post-buckled regime will often reveal isolated regions of stable equilibria with greater load-carrying capacity than the natural structural response. The regions are unattainable through the standard loading history because the regions are separated from the natural behaviour by energy barriers or interstitial unstable equilibria. Through modal nudging, the geometry of the baseline structure is marginally altered using the mode shape of a desired post-buckled state, so that the structure favours the desired response from the unloaded state. This approach does not induce any significant additions in mass (other than the minor increase derived from an applied curvature to a previously straight elements) and does not pose any significant drawbacks in terms of manufacturability or functionality during operation. Furthermore, it does not involve additional perturbation loads nor changes to original boundary conditions.

Throughout the manuscript we differentiate between two different types of nudges. A *modal nudge* relates to the concept of nudging a structure by applying a small change to the undeformed geometry in the form of the deformation mode of the desired equilibrium path. Alternatively, a *feature nudge* uses the dominant feature of the deformation mode corresponding to the desired equilibrium path. In both cases, the nature of these nudges is static, meaning that the original geometry of the structure is altered in the undeformed state, and no further dynamic nudges are applied throughout the loading history.

The essence of modal nudging is conceptually illustrated in Fig. 1. An idealised structure governed by unstable-symmetric branching with undesirable imperfection sensitivity (Fig. 1A), is transformed into a structure governed by stable-symmetric branching with desirable imperfection *in*sensitivity (Fig. 1B). Modal nudging also allows the design engineer to select which of the two desirable paths (left or right in Fig. 1B) the nudged structure will adopt.

2.1. Nudging procedure and model definition

The fundamental prerequisite for applying modal nudging is a comprehensive exploration of the geometrically nonlinear structural response, and numerical continuation proves to be an appropriate method for this task. Within a finite element setting, numerical continuation is often referred to as *generalised path-following* (Eriksson, 1998)—an arc-length-based incremental-iterative technique which enables the user to follow any equilibrium branch defined by a multi-parametric setting of the conservative and elastic structural problem. Herein, an in-house MATLAB-based finite element code (Groh and Pirrera, 2018a) is used, which makes use of quadratic beam elements employing the finite strain theory proposed by Reissner (1973) and formulated on a total Lagrangian basis.

On discovering a potentially desirable stable equilibrium solution beyond the first instability point of a structure, we extract the deformation mode, $\mathbf{u}_{\text{state}}$, of any state along the desirable stable branch and then use this state to alter the

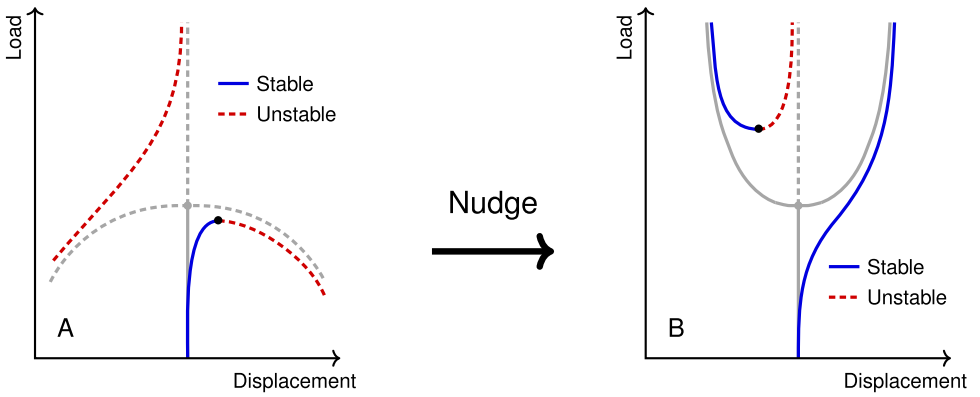

Fig. 1. Perfect and imperfect bifurcation branching responses: (A) Subcritical and (B) Supercritical.

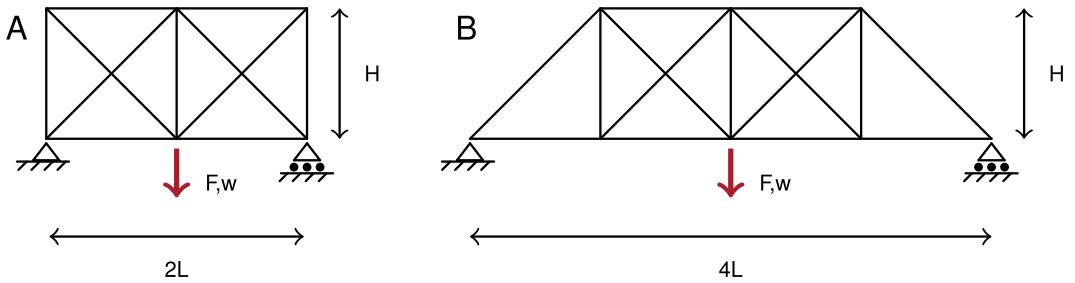

Fig. 2. Two planar frames: (A) Frame-1 and (B) Frame-2. The diagonal cross-members are not connected to each other at the points of intersection. Point load F is applied vertically downwards at midspan and the vertical displacement w is observed. All members have identical material and cross-sectional properties. The horizontal members are of the same length, L, as the vertical members, H, such that $L = H$.

original, undeformed geometry, $\mathbf{x}_0$, of the structure. Hence,

$$\mathbf{x}_{\text{nudged}} = \mathbf{x}_0 + \eta \bar{\mathbf{u}}_{\text{state}}, \tag{1}$$

with

$$\bar{\mathbf{u}}_{\text{state}} = \frac{\mathbf{u}_{\text{state}}}{\|\mathbf{u}_{\text{state}}\|_2}, \tag{2}$$

and

$$\eta \|\bar{\mathbf{u}}_{\text{state}} \oslash \mathbf{x}_0\|_2 \ll 1, \tag{3}$$

where η is the non-dimensional nudging parameter, and $\oslash$ is the Hadamard division operator defined by $C_i = A_i/B_i$ with the subscript denoting the i^{th} component of the vector. The magnitude of the nudging parameter will vary from structure to structure and from mode shape to mode shape, but for all nudges in this paper Eq. (3) holds. For a structure where Eq. (3) is not valid, the corresponding geometrical change can no longer be classified as a nudge, but rather as an entirely new structure in its own right with its own unique structural response. This latter concept is addressed further in Section 3.

Two frames are evaluated herein, frame-1 and frame-2, illustrated in Figs. 2A and 2B, respectively. For each frame, the unit cell length, L, is equal to the frame height, H, such that $L = H$. Both frames are symmetric about the vertical plane. In each case, a non-follower load, F, is applied to the bottom of the central vertical member, producing a vertical displacement, w, at the same point. Note that the structures in Fig. 2 are frame and not truss structures, meaning that joints are rigid and all members, each with identical material and cross-sectional properties, may deform in both membrane and bending action. In addition, the diagonal members are free to pass over each other and are not fixed at their intersections.

2.2. Modal nudging: Frame-1

Fig. 3A shows the load-displacement response of frame-1, with the stability of each equilibrium path highlighted (red signifies unstable equilibria; blue signifies stable equilibria). The plots are presented as non-dimensional quantities, with $\bar{F} = FL^2/Eb$ and $\bar{w} = w/L$, where E and b are Young's modulus and out-of-the-page width of each the members.

In Fig. 3A, the solutions highlighted in blue are stable equilibria and can be observed experimentally in a quasi-static loading regime. The unstable solutions highlighted in red can be computed numerically but are not readily observed experimentally because they are unstable to small perturbations. Fig. 3A also shows various branch points (B_1-B_5) and limit points

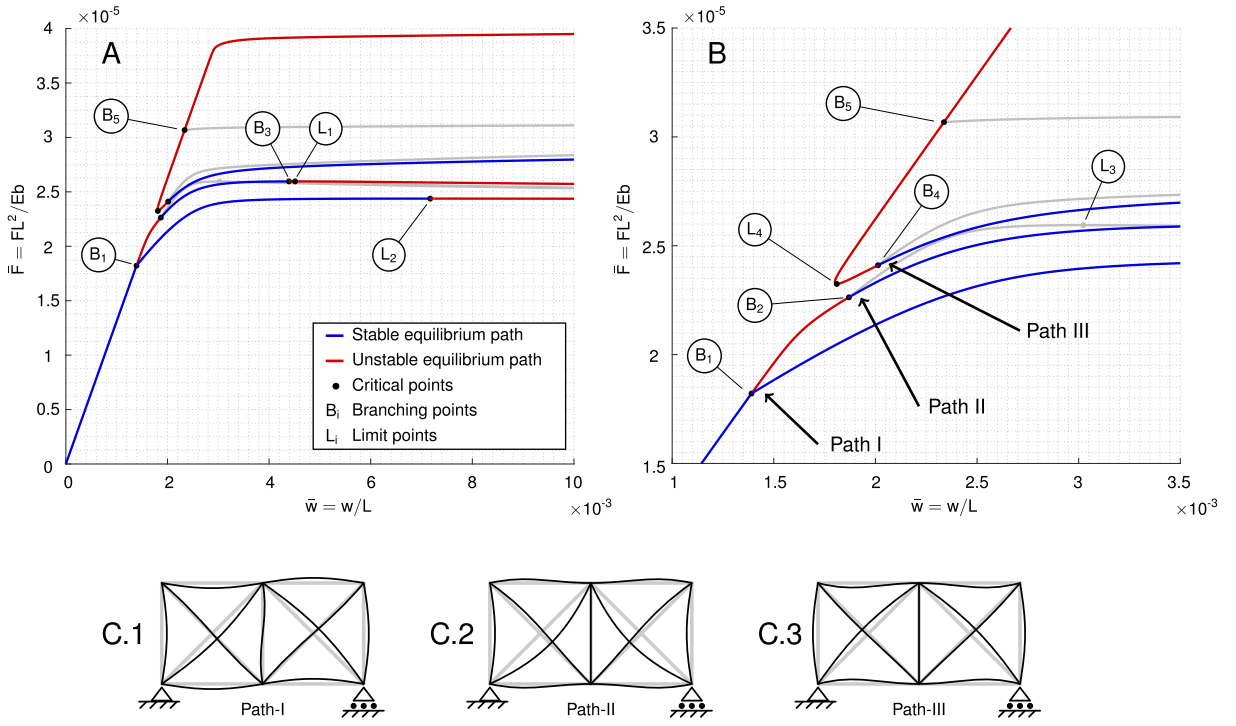

Fig. 3. (A) The non-dimensionalised load-displacement response for frame-1 with various branch and limit points highlighted as black dots. Limit points are minima and maxima, while branch points denote intersections between equilibrium paths. For clarity, some equilibrium paths emanating from branch points are shown in grey. These grey paths are unstable and each represent a unique asymmetrical deformation mode shape that is of little interest here; (B) A close-up view of (A) illustrating the three stable paths of interest (blue). Path-I is the original bifurcated asymmetric path, path-II is a desirable stable path of greater load-carrying capacity, and path-III is the highest load-carrying and most compliant stable response; (C) The deformation states observed at the beginning of each path: (C.1) path-I, an asymmetric deformation mode shape; (C.2) path-II, a symmetric deformation mode shape; (C.3) path-III, a symmetric deformation mode shape. (For interpretation of the references to colour in this figure legend, the reader is referred to the web version of this article.)

(L_1-L_4) highlighted by black dots. Limit points are minima and maxima of equilibrium paths, whereas branch points denote intersections between different equilibrium paths.

For clarity, the equilibrium plot of Fig. 3 is abridged, with a number of branched equilibrium paths plotted in grey colour. Each of these grey paths corresponds to an unstable solution, which is of little interest here and simply included for completeness. Three paths are presented in grey, a path from branch point B_4, a path from branch point B_5, and finally a path connecting branch points B_2 and B_3.

Upon loading from the unloaded state, the structure deforms linearly until the fundamentally symmetric behaviour loses stability at branch point B_1. At this point, some members of the frame buckle and the structure transitions onto the branched bifurcation path-I, which is characterised by a geometrically asymmetric deformation mode shown in Fig. 3C.1. This loading history is referred to as the *natural path*, as it describes the physical response that the structure naturally manifests under the imposed loading history. For clarity, it is important to note that although this deformation mode is geometrically asymmetric, the equilibrium path-I is in fact symmetric, that is it belongs to a symmetric pitchfork bifurcation stemming from bifurcation point B_1. This is verified by reversing the sign of $\bar{\mathbf{u}}_{\text{state}}$ in Eq. 1. The reversed structure exhibits an identical deformation mode shape to the original response, however in a mirror-image form. In other words, given the norm of the displacement field adopted here, two identical branches overlap on path-I: One corresponding to the mode shown in Fig. 3C.1 and the other one corresponding to its mirror image. To avoid confusion, we henceforth refer exclusively to the symmetry and asymmetry of the deformation mode, not of the equilibrium path.

The response illustrated in Fig. 3 is particularly interesting because two additional stable equilibrium paths (path-II and path-III) exist, which are capable of carrying greater load than the natural path-I. Path-II corresponds to the post-critical behaviour of the fundamental path, which initially destabilises at branch point B_1 but then restabilises at branch point B_2. As expected, the corresponding deformation mode shown in Fig. 3C.2 is symmetric. This equilibrium path is unattainable by means of the current loading regime, due to the interstitial unstable region between B_1 and B_2. Path-III also corresponds to a symmetric deformation mode as shown in Fig. 3C.3. In this instance, however, the path is an entirely new equilibrium path that is detached from the fundamental path, and hence unattainable because it is separated by an energy barrier from the fundamental response. This means that it is possible to transition between path-II and path-III, but only by means of an applied secondary load that snaps the frame from mode shape C.2 to mode shape C.3.

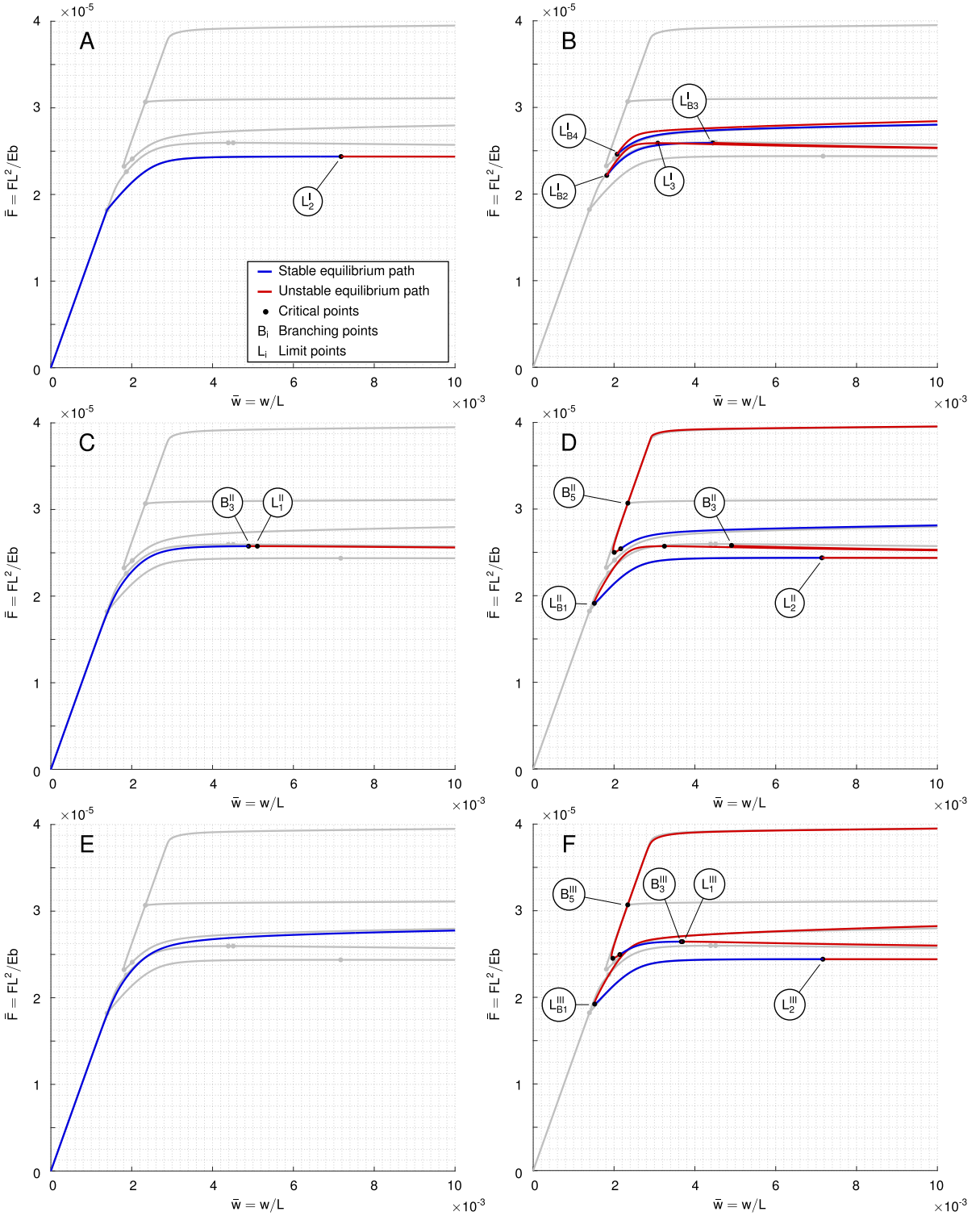

Fig. 4. The non-dimensionalised force-displacement response for the nudged frame-1. In each plot, the structural response of the baseline case is presented in grey colour. (A) Modal nudging using a path-I mode. The physical response of the baseline model is reinforced; (B) Path-II and path-III when the structure is nudged to path-I; (C) Modal nudging to path-II. With an initial geometry enforcing the symmetry of state-II, increased load-carrying capacity is observed; (D) Path-I and path-III when the structure is nudged to path-II; (E) Modal nudging to path-III. With an initial geometry enforcing the symmetry of state-III, load-carrying capacity and compliance are both increased; (F) Path-I and path-II when the structure is nudged to path-III.

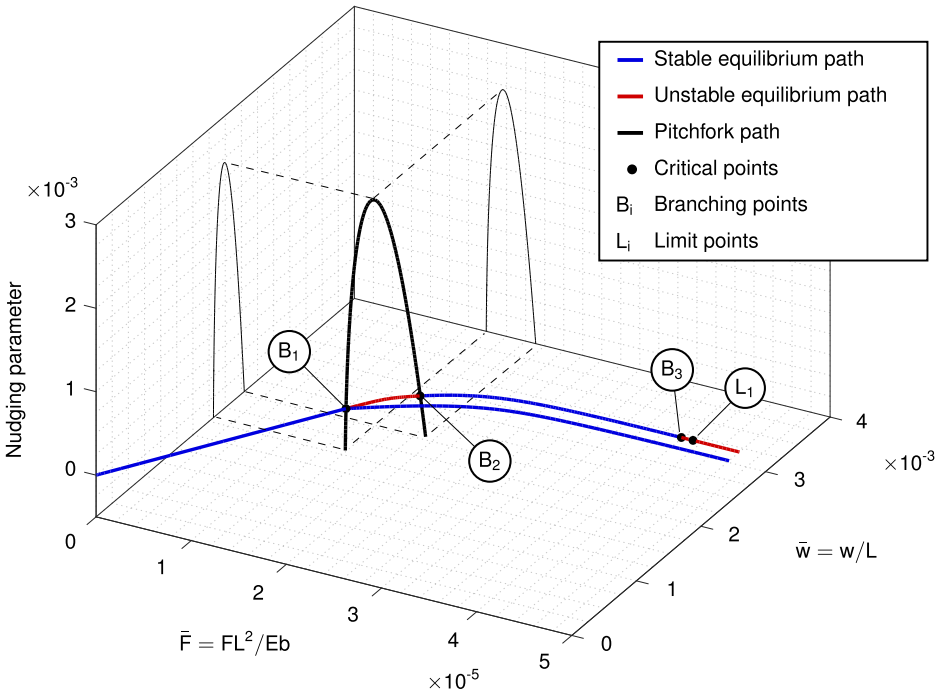

Fig. 5. A pitchfork path created by path-following the evolution of the first instability point B_1 with respect to the nudging parameter η. The pitchfork path connects branch points B_1 and B_2 and generates a cusp catastrophe at $\eta = 2.445 \times 10^{-3}$. This implies that for a nudge parameter $\eta \geq 2.445 \times 10^{-3}$ the two branch points do not exist and the natural response is given by a continuous stable path.

The idea of modal nudging is to apply a negligibly small, linearly scaled version of the deformation modes on path-II and path-III to the initial geometry of the structure (see Eq. (1)), in order to nudge it onto the respective paths and away from the natural path-I. Thus, the geometry of the structure is slightly perturbed such that path-II or path-III is energetically favourable over path-I.

Note that the mode shapes illustrated in Fig. 3C.1–3 are amplifications of the first time step after the critical point forming the path. On any equilibrium path, there exist any number of states, each corresponding to a snap-shot of the structure as it deforms. Owing to nonlinear nature of the equilibrium paths, the relative deformation between members is not constant along a specific path. With respect to modal nudging, the choice of the state used as the nudge mode is therefore significant, but not necessarily critical. In our experience, the state used in nudging can be any state along the stable paths of interest, and all states thereof will successfully cause the nudged structure to converge onto the desired path. For convenience, the nudge mode is always chosen to be the first numerically computed state after a critical point (usually a branch point), and as shown in (2), the nudge mode is always a normalised version of the chosen state.

The effect of modal nudging is presented graphically in Fig. 4, and compared directly to the original baseline response. For comparison, each plot contains additional background curves in grey colour corresponding to the original baseline response. As intuitively expected, applying modal nudging using a state from the natural path-I results in an identical overall response to the baseline. Using a nudging parameter of $\eta = 0.645 \times 10^{-3}$, the plot in Fig. 4A shows that the structure transitions smoothly from the fundamental linear path to the natural path-I in the vicinity of B_1. For general reference, a nudging parameter of $\eta = 0.645 \times 10^{-3}$ results in a maximum geometric alteration of only $\bar{u}_\eta = 1.5 \times 10^{-3}$ at the upper right corner of the frame, normalised with respect to the unit span L ($\bar{u}_\eta = \max(\eta|\mathbf{u}_{\text{state}}|)/L$).

The symmetry-breaking branch point B_1 disappears in Fig. 4A because modal nudging has broken this geometric symmetry group from the beginning. This behaviour is akin to the well-known broken-pitchfork response shown in Fig. 1. For clarity, the broken-away portion of the equilibrium path is shown in Fig. 4B. This figure illustrates the effects of path-I nudging on the response of path-II and path-III. In particular, branch point B_2 of the baseline response vanishes, leading to a broken pitchfork with a limit point L^{I}_{B2}. Thus, path-II is now unconnected from the fundamental path in the same manner as shown in Fig. 1. Similarly, for path-III the branch point B_4 has vanished and has formed a limit point L^{I}_{B4}.

The critical response for the path-I-nudged geometry is identical to the un-nudged structure. For both structures, the critical non-dimensionalised load-carrying capacity is $\bar{F} = 2.438 \times 10^{-5}$ at a critical non-dimensional displacement of $\bar{w} = 7.17 \times 10^{-3}$. As the applied nudge mode is from the natural path, the nudging parameter value required is relatively small. Selecting other states along path-I results in the same structural response, but deformation modes further along path-I, *i.e.* for greater deformation magnitudes, result in greater sensitivity to the nudge mode. This phenomena is attributed to

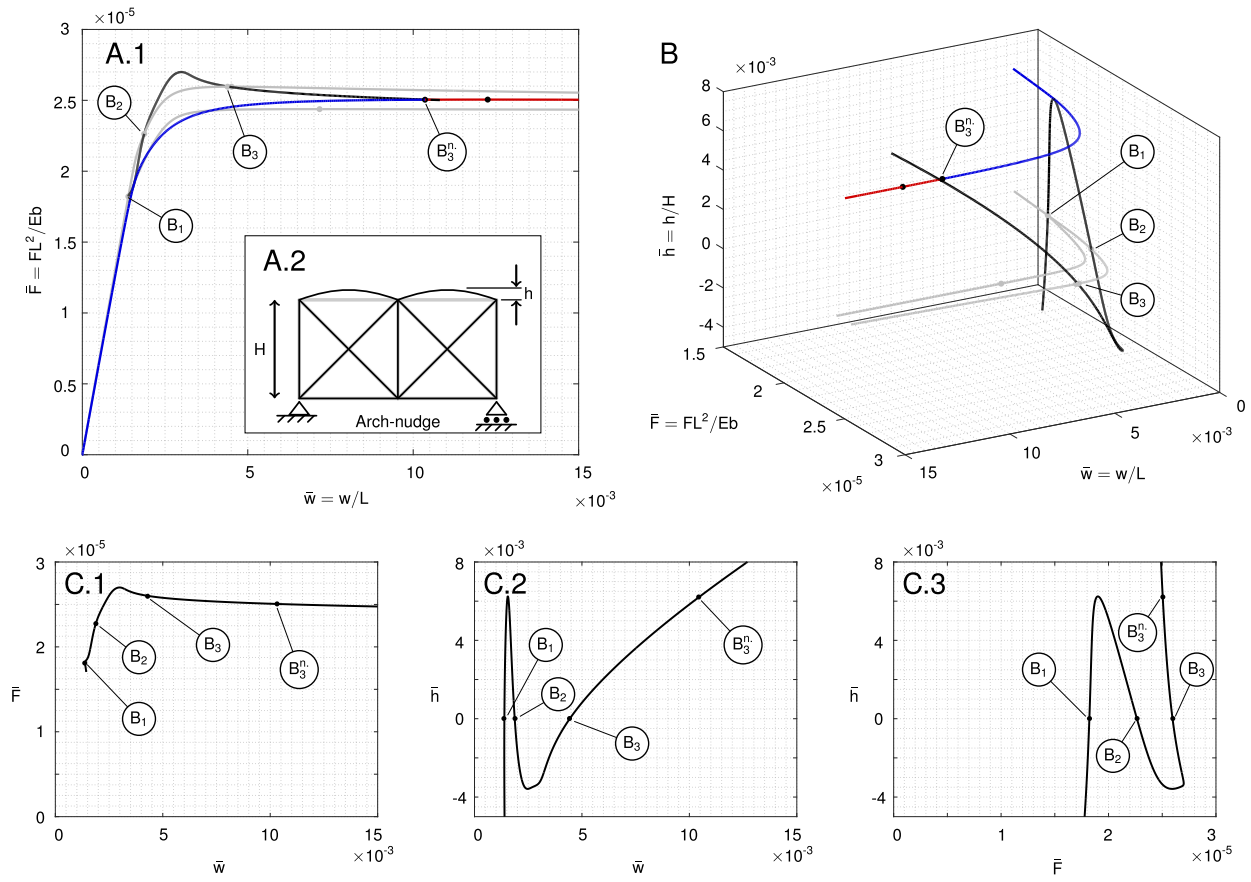

Fig. 6. (A.1) The non-dimensionalised load-displacement response for the feature-nudged frame-1, where the grey-coloured plot is an abridged version of the baseline frame response, namely path-I and path-II from Fig. 3B. The black curve is a pitchfork path which tracks branch point B_1 as the feature-nudge parameter is varied. This pitchfork path connects branch points B_1, B_2 and B_3; (A.2) A schematic diagram of the frame highlighting the feature nudge used in this instance, where h is the circular arch rise applied of the top two horizontal members; (B) A figure illustrating the same results as (A.1) as a 3D projection in load *vs.* displacement *vs.* parameter space. The parameter is the magnitude of the applied non-dimensionalised feature nudge $\bar{h} = h/H$. A value of $\bar{h} = 0$ corresponds to two flat members, which recovers the original response of the baseline frame-1. A negative value of $\bar{h} < 0$ indicates a feature nudge of inverted arches, thus concave instead of the illustrated convex; (C.1) The pitchfork curve as an orthonormal projection in load-displacement space; (C.2) The pitchfork curve as an orthonormal projection in parameter-displacement space; (C.3) The pitchfork curve as an orthonormal projection in parameter-load space.

the fact that the relative magnitude of the critical eigenvector corresponding to branch point B_1 increases the further we progress along path-I.

Fig. 4C illustrates nudging to path-II using a nudging parameter value of $\eta = 2.445 \times 10^{-3}$. The maximum geometric alteration, $\bar{u}_\eta$, for nudging to path-II is found at the upper corner of the frame. For a nudging parameter value of $\eta = 2.445 \times 10^{-3}$, this results in $\bar{u}_\eta = 5.5 \times 10^{-3}$, *i.e.* a geometric alteration of 0.55% with respect to the member length L of the baseline geometry. This nudged geometry results in a new fundamental path, which follows the baseline path-II and also removes the first symmetry-breaking branch point B_1. As a result, the path-II-nudge has stabilised the previously unstable equilibria beyond B_1, thereby capturing the previously unattainable load-carrying capacity of path-II. The critical non-dimensional load of this nudged frame is $\bar{F} = 2.576 \times 10^{-5}$ (at branch point B_3^{II})—a 5.7% increase in load-carrying capacity compared to the baseline geometry. However, the compliance of the nudged structure is almost halved compared to the baseline, from $\bar{w} = 7.18 \times 10^{-3}$ (at L_2) to $\bar{w} = 4.90 \times 10^{-3}$ (at B_3^{II}).

The effect of a path-II-nudge on the remaining two stable paths, path-I and path-III, are shown in Fig. 4D. Path-III remains largely unaffected, apart from the minor increase in load at its lower-most limit point. Similar to the path-I-nudge, nudging to path-II also removes the first branch point B_1. For the path-I-nudge, this occurs because the applied geometric alteration breaks the symmetry group associated with branch point B_1, and therefore leads to the classic case of a broken pitchfork exhibited by imperfect structures. For the path-II-nudge, branch point B_1 disappears because the geometric alteration of the nudge mode enforces symmetry and therefore makes it energetically unfavourable for the structure to break this symmetry group. Indeed, the path-II-nudge applies a slight upwards curvature to the top two horizontal members, thereby preventing the asymmetric deformation originally initiated by branch point B_1. The removal of branch point B_1 therefore forms a limit point L_{B1}^{II} on a broken-away path-I, which now creates a connection back to path-II via branch point B_3^{II}.

Depending on the magnitude of the nudging parameter, nudging to path-II can result in different behaviour. Fig. 5 shows a black pitchfork path that illustrates the evolution of branch points B_1 and B_2 of the un-nudged baseline frame as the nudging parameter for path-II is increased. For the baseline frame, branch points B_1 and B_2 signify the delimiting boundary points of the interstitial unstable region, which prevents the structure from naturally converging onto path-II. The pitchfork path shows that the applied nudge causes branch points B_1 and B_2 to converge and then annihilate at a cusp catastrophe. Hence, for a specific magnitude of the nudge mode, $\eta \geq 2.445 \times 10^{-3}$ branch points B_1 and B_2 vanish, the unstable region is removed and we recover the structural response illustrated in Fig. 4C. For values of $\eta < 2.445 \times 10^{-3}$, the unstable region remains, suggesting that a critical magnitude of the nudge mode needs to be imposed for this design strategy to work as desired.

From Fig. 4E it is evident that path-III provides the most attractive potential for modal nudging because it increases the stable load-carrying capacity and also results in the most compliant response. Hence, bridging the energy barrier between path-II and path-III uncovers the entire latent functional capacity of this particular structure. In order to erode the energy barrier, the required nudging parameter value of $\eta = 11.380 \times 10^{-3}$ is somewhat larger than for the previous two nudges. Nevertheless, the maximum geometric alteration of $\bar{u}_\eta = 25.6 \times 10^{-3}$, once again corresponding to a resultant displacement applied to the node at the upper corner of the frame, remains benign corresponding to a 1.28% change in the lateral dimension of the original structure. The results in Fig. 4E show the complete removal of all critical points, and thus no sign of instability. Indeed, the stable equilibrium path continues beyond the limits of practical elasticity and it is therefore prudent to appreciate the limitations of such compliance. The limits of the elastic regime with particular reference to strain is discussed in Section 2.5.

The remaining two stable paths, path-I and path-II, are also affected by the applied nudge to path-III, and the results are illustrated in Fig. 4F. On first viewing, it seems that the response of path-I and path-II is unchanged, but on closer inspection it is clear that path-I now connects to the path which originally bifurcated from B_4 (shown in grey in Fig. 3B). For path-II, the stable region is elevated above the previous load-carrying capacity, as illustrated by the shift away from the underlying grey baseline solution. This shift has also enabled a connection to the unstable region of path-III.

2.3. Feature nudging: Frame-1

One potential drawback of the modal nudging procedure outline in the previous section is that manufacturing a frame with the exact geometry of the mode shape required could be costly and/or complicated. This could particularly be the case as alterations to the geometry are of the order of 1–2% of the dominant original length scale. In this regard, an alternative approach to modal nudging is a feature nudge. In this instance, a dominant feature from the desirable deformation mode shape is used as a nudging parameter. For example, consider the deformation mode for path-II (Fig. 3C.2). The differentiating feature between the mode shape along path-II and the natural mode of path-I (Fig. 3C.1) is primarily the symmetric convex deformation of the top two horizontal members. Hence, rather than using the full mode shape, this particular feature can be used to nudge the structure onto path-II. The goal of feature nudging is once again to enforce symmetry from the outset and therefore remove the symmetry-breaking branch point B_1. In applying an initial convex curvature to the top two members of the frame, a symmetry-breaking equilibrium path may still exist, but it will be separated by an energy barrier from the fundamental symmetry-preserving solution.

The feature nudge explored here maintains the overall geometry of the frame, but introduces two circular arches as the top two members of the frame (Fig. 6A.2). The magnitude of the applied feature nudge is measured by the non-dimensionalised arch height $\bar{h} = h/H$, where h is the midpoint rise of the arches. As shown in Fig. 6A.1, the feature nudge bridges the unstable interstitial region between branch points B_1 and B_2 and therefore enables the full exploitation of path-II. However, it is also clear from Fig. 6A.1 that the feature-nudged response does not overlap with the un-nudged baseline path-II shown in grey. Hence, a feature nudge is not as effective as a modal nudge, because it does not exploit the full mode shape to nudge the structure onto the desired equilibrium path. This also means that the feature nudge requires a greater magnitude of the nudge parameter to be effective.

Using the capabilities of generalised path-following it is possible to trace the evolution of branch points B_1 and B_2 *vs* the feature-nudge parameter. Thus, a locus of points tracing these branch points is solved in $F - w - \bar{h}$ space, as shown by the black curve in Fig. 6. The 3D plot of this curve in Fig. 6B, and the orthonormal projections in C.2 and C.3, show that these two branch points converge and then annihilate at a cusp catastrophe for $\bar{h} = 6.25 \times 10^{-3}$. This means that for a feature nudge with arch rise of $\bar{h} \geq 6.25 \times 10^{-3}$, the unstable region on path-II is removed and a greater load-carrying capacity than the natural path-I is achieved. Most importantly, this enhanced load-carrying capacity is achieved with minimal addition in mass. Any increase in mass is entirely due to the greater arc-length of the arches compared to the flat members, but for a rise-to-span ratio of 0.6%, this mass penalty is negligible.

Interestingly, Fig. 6C.3 illustrates a double cusp behaviour at $\bar{h} = 6.25 \times 10^{-3}$ and $\bar{h} = -3.55 \times 10^{-3}$. For upwards facing arches with $\bar{h} \geq 6.25 \times 10^{-3}$ branch point B_1 and B_2 vanish and only branch point B_3 remains. Similarly, for downwards facing arches with $\bar{h} \leq -3.55 \times 10^{-3}$ branch points B_2 and B_3 vanish and only branch point B_1 remains. For any intermediate arch configuration $-3.55 \times 10^{-3} \leq \bar{h} \leq 6.25 \times 10^{-3}$ all three branch points exist. Hence, this behaviour illustrates the general double cusp feature of the swallowtail catastrophe.

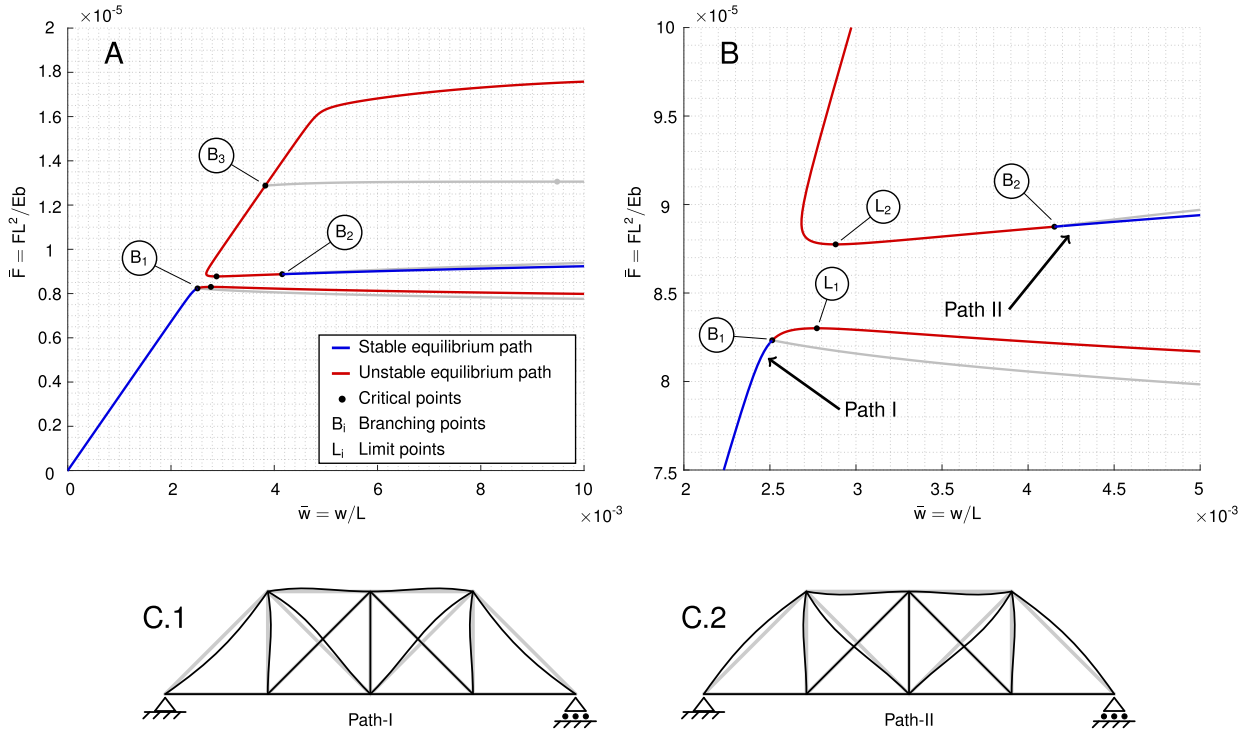

Fig. 7. (A) The non-dimensionalised load-displacement response for frame-2, where a number of paths emanating from branch points are shown in grey colour. These grey paths are unstable and each represents a unique asymmetrical deformation mode shape that is of little interest to the techniques used herein. The other colours used represent the stability of the associated equilibrium curves: red & grey, unstable; blue, stable. The critical points, both for branch points and limit points, are represented by black dots; (B) An enlarged view of (A) illustrating the two paths of interest, path-I and path-II. Path-I is the natural response leading to structural collapse at branch point B_1, and path-II is a more desirable equilibirum path of greater load-carrying capacity and compliance. For the baseline frame-2, this response is physically unattainable under the displayed loading regime because it is separated from path-I by an energy barrier; (C) The deformation states observed at the beginning of each path: (C.1) corresponds to path-I, a symmetric deformation mode shape; (C.2) to path-II, also a symmetric deformation mode shape. Note that the fundamental path restabilises after a sufficiently large displacement, but this portion of the curve is not shown here as it is well into the materially inelastic region. (For interpretation of the references to colour in this figure legend, the reader is referred to the web version of this article.)

2.4. Modal nudging: Frame-2

Frame-2 geometrically extends frame-1 by adding four additional members to the length of the overall frame (see Fig. 2B). Fig. 7 illustrates the non-dimensional load-displacement response of frame-2 with the stability of equilibria highlighted in colour (red, unstable; blue, stable; grey, unstable and of little importance for modal nudging).

The load-displacement plot in Fig. 7A shows a predominantly linear pre-buckling path, which results in an unstable post-buckling behaviour at the first branch point B_1. Owing to the subcritical nature of this branch point, frame-2 would snap into a remote stable region of the fundamental path upon reaching B_1, but because this portion of the curve is well into the materially inelastic region it is not shown here. Hence, restricting the desirable behaviour to elasticity, the baseline frame-2 is assumed to collapse and fail at B_1. However, frame-2 features a stable equilibrium path-II of greater load-carrying capacity, which is disconnected from the natural path-I by an energy barrier. The deformation mode shapes of path-I and path-II are presented in Fig. 7C.1 and C.2, respectively. By seeding a small proportion of mode C.2 to the baseline geometry of frame-2, it is possible to nudge the structure onto the equilibrium path of greater load-carrying capacity.

Indeed, Fig. 8 illustrates a successful modal nudge to path-II for an applied nudge parameter of $\eta = 1.375 \times 10^{-3}$. The benefits of modal nudging for this frame extend beyond a mere increase in load-carrying capacity and compliance. In this case, nudging has facilitated a clear transition in structural response from a subcritical pitchfork instability, with associated undesirable imperfection sensitivity, to a geometrically nonlinear softening response with imperfection *in*sensitivity within the elastic range. To make sure that the observed gains in load-carrying capacity and compliance are actually achievable, we evaluate the associated strains throughout the deformation regime.

2.5. Elastic response of frames 1 and 2

For all of the analyses undertaken herein, an assumption of linear elasticity (small strains) has been made. This is a valid assumption especially for the linear pre-buckling behaviour where the frame behaves in a stiff linear manner. As modal

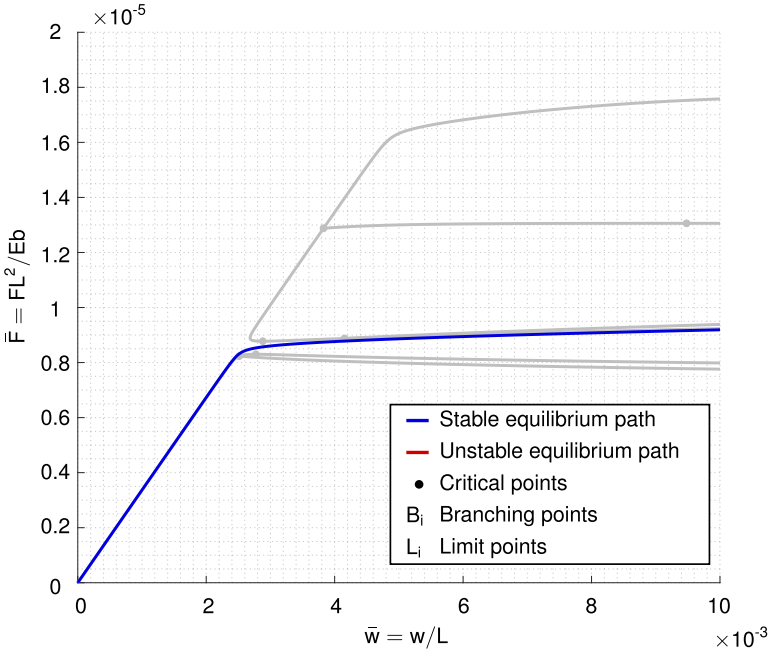

Fig. 8. The non-dimensionalised force-displacement response for the nudged frame-2. For reference, the structural response of the baseline frame is presented in grey colour. Modal nudging to path-II results in increased load-carrying capacity, increased compliance and imperfection insensitivity.

Table 1
Non-dimensionalised loads and displacements for certain strain limits and first instability points for frame-1 and frame-2.

		1%	2%	3%	4%	5%	6%	Instability
Frame 1 (Baseline)	$\bar{F}$ [$\times 10^{-5}$]	1.925	2.302	2.417	2.433	2.437	–	2.438
	$\bar{w}$ [$\times 10^{-3}$]	1.58	2.45	3.41	4.48	5.88	–	7.17
Frame 1 (Nudge-I)	$\bar{F}$ [$\times 10^{-5}$]	1.959	2.312	2.418	2.434	2.437	–	2.438
	$\bar{w}$ [$\times 10^{-3}$]	1.64	2.49	3.46	4.58	5.96	–	7.18
Frame 1 (Nudge-II)	$\bar{F}$ [$\times 10^{-5}$]	2.130	2.522	2.569	–	–	–	2.576
	$\bar{w}$ [$\times 10^{-3}$]	1.75	2.86	3.84	–	–	–	4.90
Frame 1 (Nudge-III)	$\bar{F}$ [$\times 10^{-5}$]	2.142	2.596	2.675	2.715	2.745	2.773	–
	$\bar{w}$ [$\times 10^{-3}$]	1.73	2.92	4.00	5.45	7.30	9.68	–
Frame 2 (Baseline)	$\bar{F}$ [$\times 10^{-6}$]	–	–	–	–	–	–	8.233
	$\bar{w}$ [$\times 10^{-3}$]	–	–	–	–	–	–	2.51
Frame 2 (Nudge-II)	$\bar{F}$ [$\times 10^{-6}$]	8.543	8.791	8.994	9.208	9.424	9.652	–
	$\bar{w}$ [$\times 10^{-3}$]	2.80	4.25	6.71	10.35	14.92	20.57	–

nudging increases the compliance of the frames, and the post-critical response is governed by reduced structural stiffness, it is possible that the elastic strain limit is exceeded throughout the post-buckling regime. Fig. 9A, B and C illustrate the observed strains throughout the loading regime for nudges to path-I, path-II and path-III of frame-1. Fig. 9D illustrates the observed strains for nudging frame-2 to path-II.

The strain limit to be imposed is a function of the material system used. In this regard, the reader is directed to Hao et al. (2013), where a range of large-strain elastic materials are evaluated for their performance. The materials presented therein allow for strains in the order of 6–7%, *e.g.* $< 1\%$ for steels, 0.5-2.5% for Titanium alloys, 2–3% for Gum metals, and as high as 6–7% for NICSMA (nanowire *in situ* composite with shape-memory alloy). Integer values of these strain limits in the range of [1, 7]% are marked on the equilibrium curves of Fig. 9. These strain limits show that, for the frames considered here, modal nudging can lead to an appreciable increase in functionality if strains greater than 1% can be tolerated. This response is naturally also a function of the ratio of second moment of area to cross-sectional area of the frame members. As this ratio decreases, buckling failure of individual members will occur relatively earlier compared to strain-limit failure, and therefore enable greater benefits from modal nudging. Hence, modal nudging may be particularly attractive for MEMS devices.

In conjunction with Fig. 9, the strain values, and their corresponding non-dimensionalised loads and displacements, are presented in Table 1, which provides a summary of the improved functionality enabled by modal nudging. For frame-2, the un-nudged baseline response exhibits an instability before an imposed strain of 0.7%. Modal nudging to path-II results in an

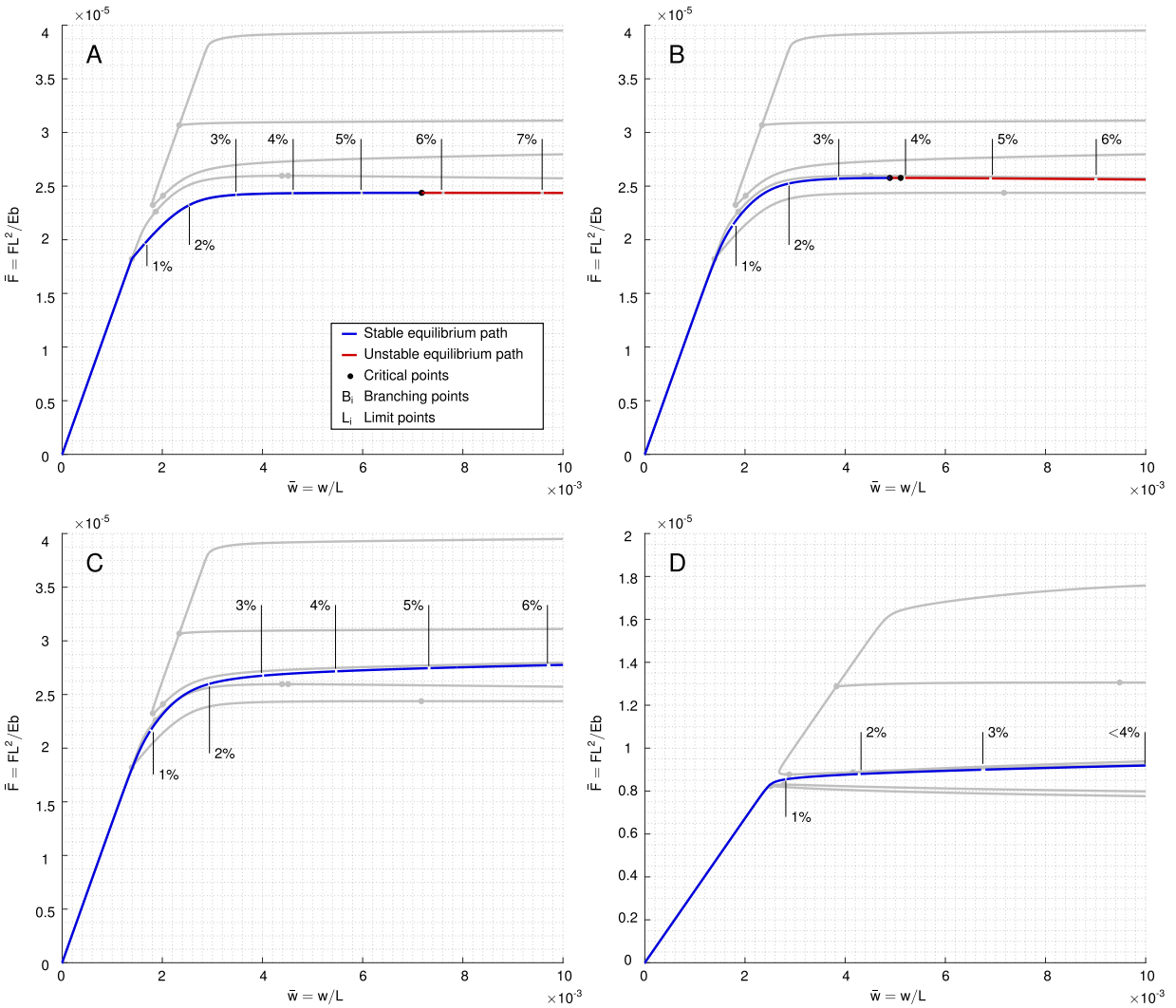

Fig. 9. Load-displacement response for modal nudging of frame-1 and frame-2, highlighting the observed strains throughout the loading history. The baseline un-nudged response is illustrated in grey colour, and the nudged response curves differentiate between blue curves (stable equilibria) and red curves (unstable equilibria). (A) Frame-1 nudged to path-I; (B) Frame-1 nudged to path-II; (C) Frame-1 nudged to path-III; (D) Frame-2 nudged to path-II. (For interpretation of the references to colour in this figure legend, the reader is referred to the web version of this article.)

increase in load-carrying capacity of 3.7% and an increase in compliance of 11.6% at an imposed strain limit of 1%. Thus, for frames whose material remains elastic for small to moderate strains, modal nudging could provide (i) an increase in load-carrying capacity, and (ii) a means of transforming subcritical pitchfork bifurcations into supercritical pitchfork bifurcations. For more novel applications, such as MEMS devices that use high-performance NICSMA metals with an elastic strain limit of 6%, modal nudging increases the load-carrying capacity of frame-2 by 17.24% and the compliance by 719.5% over the baseline response.

3. Limitations of modal nudging

In this section, two additional frames are analysed to show some of the limitations of modal nudging. Frame-3 and frame-4 are presented in Fig. 10, which are both similar to frame-2 apart from the removal of one of the diagonal members. The non-dimensionalised load-displacement response of frame-3 and frame-4 are shown in Figs. 11A and 11 B, respectively. These equilibrium curves show that both frames do not present an opportunity for modal nudging to a more desirable structural response, because no additional stable equilibrium paths exist in the elastic post-critical regime. Note again that some of the equilibrium paths restabilise at limit points sufficiently deep in the post-buckling regime. However, the large deformations associated with these states means that the materials have crossed the boundary to plasticity. These modes are

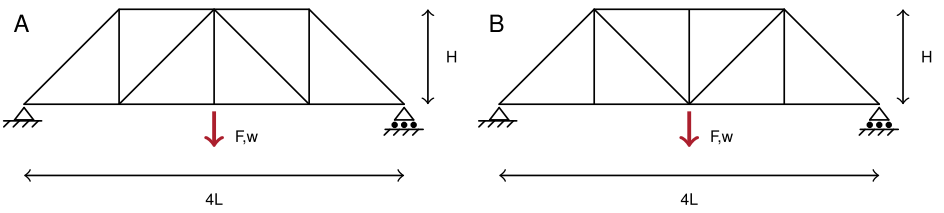

Fig. 10. Two frames exhibiting reduced structural redundancy. (A) Frame-3; (B) Frame-4. Both frames are similar to frame-2, but in both cases one of two diagonal members has been removed. A load F is applied vertically downward and the vertical displacement w is observed. All members have identical material properties and rectangular cross-sections.

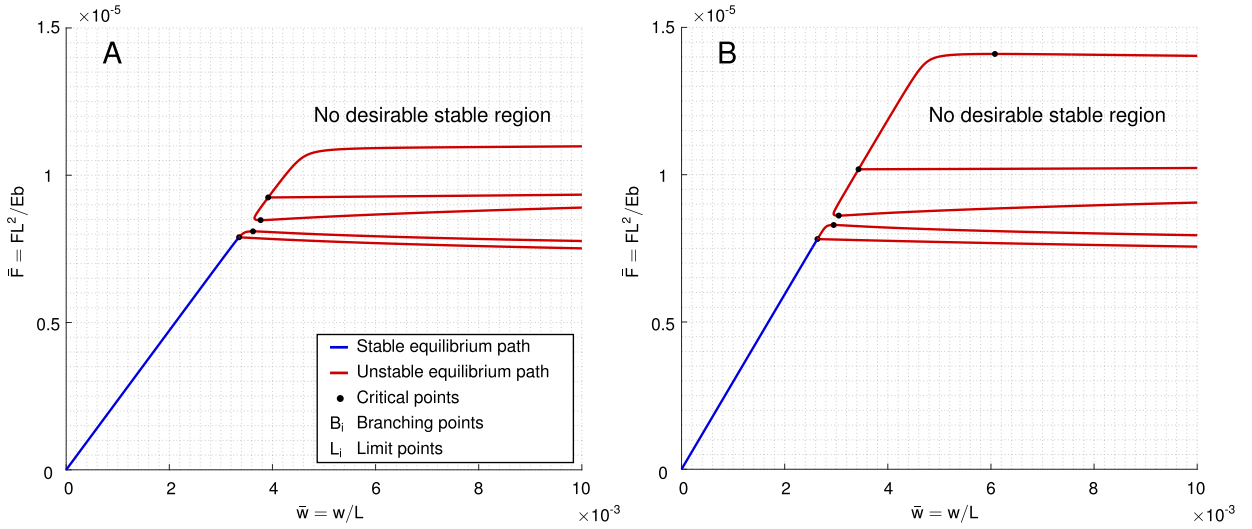

Fig. 11. Frames exhibiting reduced structural redundancy, such that there exists no stable equilibrium solutions in the elastic post-critical regime beyond the initial point of instability. (A) Load-displacement response for frame-3; (B) Load-displacement response for frame-4. Note that the fundamental path restabilises deep in the post-buckling region, but because this is associated with non-reversible plastic deformations it is not shown here.

not useful in terms of modal nudging and also mean that for practical purposes the baseline structure fails upon reaching the first instability point.

The absence of additional stable equilibria in the post-critical regime can be defined as a reduction of structural redundancy. Hence, once the first member of frame-3 and frame-4 buckles, both structures will collapse. This reduced structural redundancy is related to the removal of one of the diagonal members, which in case of frame-2, provides the requisite means for redistributing load paths and therefore endows the structure with post-critical load-carrying capacity.

The authors have, nevertheless, attempted to nudge frame-3 and frame-4 to unstable equilibrium paths. In this case, no improvements in load-carrying capacity were possible. An interesting feature, however, was the ability to use large values of the nudging-parameter, η, to fundamentally change the geometry of the frames (as opposed to a small nudge-mode imperfection) leading to very compliant structures. These compliant structures pose little resemblance to the baseline frames and essentially act as large springs; essentially, converging to stable solutions from deep within the post-critical regime, thus making use of deformations which are equal to the magnitude of the baseline frame or even greater.

For completeness, it is also noted that conventional structures are often subjected to multiple loading cases. The current nudge may in fact trigger less desirable modes for other load cases. Therefore, nudging a structure for one load case could potentially reduce the load-carrying capacity for other load cases. The authors are yet to investigate this phenomena as it falls outside the scope of the current work.

The implications for modal nudging are therefore clear. Significant improvements in load-carrying capacity, compliance or imperfection sensitivity are only possible if some degree of structural redundancy, by means of post-critical load re-distribution, is possible. Indeed, a general rule of thumb for optimising structures is the notion that reducing redundancy improves efficiency. For structures designed in the linear regime this may ultimately be true. For structures that attempt to exploit nonlinearities, however, reducing or removing structural redundancy may not only lead to post-critical collapse, but also remove the opportunity to further tailor the structural response via modal nudging.

4. Conclusion

A new structural optimisation technique, referred to as *modal nudging*, has been introduced. Although optimisation techniques such as precambering (Su and Wang, 2012) and prestressing (Saito and Wadee, 2007) are used widely to increase the load-carrying capacity of frames, modal nudging is unique in that it uses deformation mode shapes from stable equilibria in the post-buckling regime to alter the baseline geometry and tailor the structure's post-buckling response. This technique has shown great potential to optimise nonlinear structures for (i) increased load carrying capacity; (ii) compliance; and (iii) the design of imperfection-insensitive structures. Equally, the technique may be used as a means of modal differentiation for shape-adaptive technologies that employ buckling instabilities to transition between a number of different configurations.

This paper shows that the mechanical behaviour of nonlinear frame structures that possess structural redundancies—by means of additional load-carrying capacity in the post-buckling regime—is very rich. Previously unseen stable equilibrium paths of greater load-carrying capacity are presented for the first time, which include equilibria that are separated from the fundamental response of the frame by energy barriers. We have shown that the frames can be nudged onto these higher load-carrying paths by marginally perturbing the baseline geometry. The nudged response to these paths generally leads to a stable structural response with increased compliance, increased load-carrying capacity and reduced imperfection sensitivity.

A key factor for the successful application of modal nudging is the concept of structural redundancy. This term is used to refer to structures which possess the means to redistribute loads to additional regions of stability in the post-buckling regime; particularly to isolated stable regions separated from the fundamental structural response by interstitial unstable equilibria, or alternatively, energy barriers. If these conditions are met, then the structure may exhibit latent load-carrying capacity, which can be readily exploited via modal nudging.

The results presented explicitly for frame structures herein, are applicable from the micro- to the macro-scale, and may thus lead to similar studies throughout a wide range of scientific disciplines that deal with nonlinearities. Future work will focus on demonstrating the capabilities of modal nudging on cylindrical shell structures; both for increasing traditional load-carrying and for modal differentiation in smart shape-adaptive applications.

Acknowledgements

BSC is supported by the UK Engineering and Physical Sciences Research Council (EPSRC) through the EPSRC Centre for Doctoral Training in Advanced Composites for Innovation and Science [grant number EP/G036772/1], AP is supported by the EPSRC through their Fellowship Scheme [grant number EP/M013170/1], and RMJG is supported by the Royal Academy of Engineering under the Research Fellowship scheme [grant number RF/201718/17178].

Data statement

All data required to reproduce the figures in this paper can be found on the data repository of the University of Bristol via URL: https://doi.org/10.5523/bris.26bgg8ae8t05o2jzwp689nic4x.

References

Andò, B., Baglio, S., Trigona, C., Dumas, N., Latorre, L., Nouet, P., 2010. Nonlinear mechanism in mems devices for energy harvesting applications. J. Micromech. Microeng. 20 (12), 125020.

Arbocz, J., Hol, J., 1995. Collapse of axially compressed cylindrical shells with random imperfections. Thin-Walled Struct. 23 (1), 131–158. doi:10.1016/0263-8231(95)00009-3.

Arena, G., Groh, R.M.J., Brinkmeyer, A., Theunissen, R., Weaver, P.M., Pirrera, A., 2017. Adaptive compliant structures for flow regulation. Proc. R. Soc. A: Math., Phys. Eng. Sci. 473 (2204), 20170334. doi:10.1098/rspa.2017.0334.

Bertoldi, K., Reis, P.M., Willshaw, S., Mullin, T., 2010. Negative Poisson's ratio behavior induced by an elastic instability. Adv. Mater. 22, 361–366.

Bogue, R., 2013. Recent developments in mems sensors: a review of applications, markets and technologies. Sensor Revi. 33 (4), 300–304. doi:10.1108/SR-05-2013-678.

Burgueño, R., Hu, N., Heeringa, A., Lajnef, N., 2014. Tailoring the elastic postbuckling response of thin-walled cylindrical composite shells under axial compression. Thin-Walled Struct. 84, 14–25. doi:10.1016/j.tws.2014.05.009.

Cox, B.S., Groh, R.M.J., Avitabile, D., Pirrera, A., 2018. Exploring the design space of nonlinear shallow arches with generalised path-following. Finite Elem. Anal. Des. 143, 1–10. doi:10.1016/j.finel.2018.01.004.

Eriksson, A., 1998. Structural instability analyses based on generalised path-following. Comput. Methods Appl. Mech. Eng. 156, 45–74.

Florijn, B., Coulais, C., van Hecke, M., 2014. Programmable mechanical metamaterials. Phys. Rev. Lett. 113, 175503.

Gomez, M., Moulton, D.E., Vella, D., 2017. Passive control of viscous flow via elastic snap-through. Phys. Rev. Lett. 119, 144502.

Groh, R., Pirrera, A., 2018. Generalised path-following for well-behaved nonlinear structures. Comput. Methods Appl. Mech. Eng. 331, 394–426. http://www.sciencedirect.com/science/article/pii/S0045782517307521.

Groh, R., Pirrera, A., 2018b. Orthotropy as a driver for complex stability phenomena in cylindrical shell structures, *Composite Structures* (Under Review).

Hao, S., Cui, L., Jiang, D., Han, X., Ren, Y., Jiang, J., Liu, Y., Liu, Z., Mao, S., Wang, Y., Li, Y., Ren, X., Ding, X., Wang, S., Yu, C., Shi, X., Du, M., Yang, F., Zheng, Y., Zhang, Z., Li, X., Brown, D.E., Li, J., 2013. A transforming metal nanocomposite with large elastic strain, low modulus, and high strength. Science 339 (6124), 1191–1194. doi:10.1126/science.1228602.

Harne, R., Wang, K., 2013. A review of the recent research on vibration energy harvesting via bistable systems. Smart Mater. Struct. 22, 023001.

Hu, N., Burgueño, R., 2017. Harnessing seeded geometric imperfection to design cylindrical shells with tunable elastic postbuckling behavior. J. Appl. Mech. 84, 011003.

Hu, N., Burgueño, R., Lajnef, N., 2014. Structural optimization and form-finding of cylindrical shells for targeted elastic postbuckling response. In: Proceedings of the ASME 2014 Conference on Smart Materials, Adaptive Structures and Intelligent Systems.

Hu, N., Burgueño, R., 2015. Buckling-induced smart applications: recent advances and trends. Smart Mater. Struct. 24, 1. doi:10.1088/0964-1726/24/6/063001.

Hu, N., Burgueño, R., 2015. Elastic postbuckling response of axially-loaded cylindrical shells with seeded geometric imperfection design. Thin-Walled Struct. 96, 256–268. doi:10.1016/j.tws.2015.08.014.
Jiménez, F.L., Marthelot, J., Lee, A., Hutchinson, J.W., Reis, P.M., 2017. Technical brief: knockdown factor for the buckling of spherical shells containing large-amplitude geometric defects. J. Appl. Mech. 84 (3), 034501–034504. doi:10.1115/1.4035665.
Jog, C.S., Patil, K.D., 2016. A hybrid finite element strategy for the simulation of mems structures. Int. J. Numer. Methods Eng. 106, 527–555.
Leggett, W., 2014. The politics of behaviour change: nudge, neoliberalism and the state. Policy Politics 42 (1), 3–19. doi:10.1332/030557312X655576.
Mang, H.A., Schranz, C., Mackenzie-Helnwein, P., 2006. Conversion from imperfection-sensitive into imperfection-insensitive elastic structures. i: theory. Comput. Methods Appl. Mech. Eng. 195, 1422–1457.
Mullin, T., Deschanel, S., Bertoldi, K., Boyce, M.C., 2007. Pattern transformation triggered by deformation. Phys. Rev. Lett. 99, 084301.
Ning, X., Pellegrino, S., 2015. Imperfection-insensitive axially loaded thin cylindrical shells. Int. J. Solids Struct. 62, 39–51. doi:10.1016/j.ijsolstr.2014.12.030.
Overvelde, J.T.B., Shan, S., Bertoldi, K., 2012. Compaction through buckling in 2D periodic, soft and porous structures: effect of pore shape. Adv. Mater. 24, 2337–2342.
Pirrera, A., Avitabile, D., Weaver, P.M., 2012. On the thermally induced bistability of composite cylindrical shells for morphing structures. Int. J. Solids Struct. 49, 685–700. doi:10.1016/j.ijsolstr.2011.11.011.
Previtali, F., Bleischwitz, R., Hasse, A., Campanile, L.F., Ermanni, P., 2011. Compliant morphing wing. In: ICAST2011: 22nd International Conference on Adaptive Structures and Technologies, Corfu, Greece.
Reis, P.M., 2015. A perspective on the revival of structural (in)stability with novel opportunities for function: from buckliphobia to buckliphilia. J. Appl. Mech. 82 (11), 111001–1–11001–4. doi:10.1115/1.4031456.
Reissner, E., 1973. On one-dimensional, large-displacement, finite strain beam theory. Stud. Appl. Math. 52, 87–95.
Saito, D., Wadee, M.A., 2007. Post-buckling behaviour of prestressed steel stayed columns. Eng. Struct. 30, 1224–1239. doi:10.1016/j.engstruct.2007.07.01.
Schranz, C., Krenn, B., Mang, H.A., 2006. Conversion from imperfection-sensitive into imperfection-insensitive elastic structures. ii: numerical investigation. Comput. Methods Appl. Mech. Eng. 195, 1458–1479.
Sofla, A.Y.N., Meguid, S.A., Tan, K.T., Yeo, W.K., 2010. Shape morphing of aircraft wing: status and challenges. Mater. Des. 31, 1284–1292. doi:10.1016/j.matdes.2009.09.011.
Su, R., Wang, L., 2012. Axial strengthening of preloaded rectangular concrete columns by precambered steel plates. Eng. Struct. 38, 42–52. doi:10.1016/j.engstruct.2012.01.003.
Thaler, R.H., 2015. Misbehaving. The making of Behavioural Economics, 2 Allen Lane.
Thaler, R.H., Sunstein, C.R., 2009. Nudge: Improving decisions about health, wealth, and happiness, 2 Penguin Books.
Thompson, J.M.T., Hunt, G.W., 1973. A General Theory of Elastic Stability. John Wiley & Sons.
Tsai, N.-C., Sue, C.-Y., 2007. Review of mems-based drug delivery and dosing systems. Sens. Actuators, A 134 (2), 555–564. doi:10.1016/j.sna.2006.06.014.
Voyer, B.G., 2015. 'Nudging' behaviours in healthcare: insight from behavioural economics. British J. Healthcare Manage. 21 (3), 130–135. doi:10.12968/bjhc.2015.21.3.130.
White, S.C., Weaver, P.M., 2016. Towards imperfection insensitive buckling response of shell structures: shells with plate-like post-buckled responses. Aeronaut. J. 120 (1224). doi:10.1017/aer.2015.14.
Wu, Z., Raju, G., Weaver, P., 2018. Optimization of postbuckling behaviour of variable thickness composite panels with variable angle tows: towards "buckle-free" design concept. Int. J. Solids Struct. 132–133, 66–79.